Available online at www.sciencedirect.com

SciVerse ScienceDirect

Journal of the European Ceramic Society 32 (2012) 1635–1642

www.elsevier.com/locate/jeurceramsoc

Evolution of hot corrosion resistance of YSZ, $Gd_2Zr_2O_7$, and $Gd_2Zr_2O_7$ + YSZ composite thermal barrier coatings in $Na_2SO_4 + V_2O_5$ at 1050 °C

M.H. Habibi, Li Wang, S.M. Guo *

Department of Mechanical Engineering, Louisiana State University, Baton Rouge, LA 70803, USA

Received 9 November 2011; received in revised form 31 December 2011; accepted 7 January 2012
Available online 29 January 2012

Abstract

This paper compares the hot corrosion performance of yttria stabilized zirconia (YSZ), $Gd_2Zr_2O_7$, and YSZ + $Gd_2Zr_2O_7$ composite coatings in the presence of molten mixture of $Na_2SO_4 + V_2O_5$ at 1050 °C. These YSZ and rare earth zirconate coatings were prepared by atmospheric plasma spray (APS). Chemical interaction is found to be the major corrosive mechanism for the deterioration of these coatings. Characterizations using X-ray diffraction (XRD) and scanning electron microscope (SEM) indicate that in the case of YSZ, the reaction between $NaVO_3$ and Y_2O_3 produces YVO_4 and leads to the transformation of tetragonal ZrO_2 to monoclinic ZrO_2. For the $Gd_2Zr_2O_7$ + YSZ composite coating, by the formation of $GdVO_4$, the amount of YVO_4 formed on the YSZ + $Gd_2Zr_2O_7$ composite coating is significantly reduced. Molten salt also reacts with $Gd_2Zr_2O_7$ to form $GdVO_4$. Under a temperature of 1050 °C, $Gd_2Zr_2O_7$ based coatings are more stable, both thermally and chemically, than YSZ, and exhibit a better hot corrosion resistance.

Keywords: B. Failure analysis; C. Corrosion; D. ZrO_2; High temperature coatings

1. Introduction

Thermal barrier coatings (TBCs) are frequently used on the blades and vanes of gas turbines to provide thermal insulation. By lowering the metal temperature in conjunction with the use of internal cooling and film cooling technology, TBC improves both component durability and engine efficiency.[1,2] TBC is comprised of a ceramic top layer and a metallic bond coat.[3,4] The most common top layer is made of yttria partially stabilized zirconia (YSZ) for reducing the temperature of the substrate, and a typical bond coat is the MCrAlY alloy, for efficiently preventing the substrate from oxidation and hot corrosion. Thermal barrier coatings can be fabricated by various processing techniques such as atmospheric plasma spray (APS), vacuum plasma spray, HVOF (High Velocity Oxygen Fuel) thermal spray, and electron beam physical vapor deposition (EB-PVD).[5] Although YSZ based TBC systems have been used widely in gas turbine industry, YSZ is prone to hot corrosion caused by molten salts, such as Na, S and V, contained in low-quality fuels at high working temperatures.[6,7] The search for alternative coating materials other than the well established YSZ system has consisted of two main approaches: (i) alternative materials to ZrO_2-based systems, and (ii) alternative stabilizers to Y_2O_3 for ZrO_2-based systems. Significantly, the $A_2B_2O_7$-type rare-earth zirconate ceramics, such as $La_2Zr_2O_7$, $Nd_2Zr_2O_7$, $Gd_2Zr_2O_7$ and $Sm_2Zr_2O_7$, have been shown recently to have lower thermal conductivity, higher melting points, relatively higher thermal expansion coefficients (TEC), higher stability, and better ability to accommodate defects than YSZ.[8–10] However, for the hot corrosion behavior of $Gd_2Zr_2O_7$ and other rare earth zirconates, most of early studies reported a testing temperature range between 650 and 900 °C on hot pressed samples. In this paper, the hot corrosion behavior of APS $Gd_2Zr_2O_7$, YSZ, and $Gd_2Zr_2O_7$ + YSZ composite coatings under $Na_2SO_4 + V_2O_5$ mixture is examined at an engine representative temperature of 1050 °C.

* Corresponding author. Tel.: +1 225 578 7619; fax: +1 225 578 5924.
E-mail address: sguo2@lsu.edu (S.M. Guo).

0955-2219/$ – see front matter © 2012 Elsevier Ltd. All rights reserved.
doi:10.1016/j.jeurceramsoc.2012.01.006

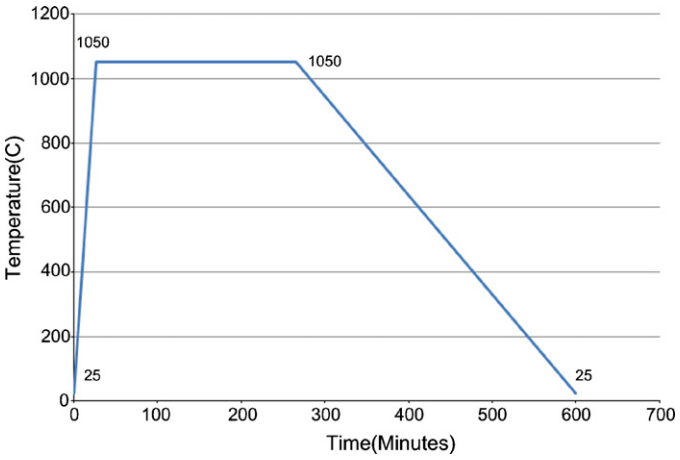

Fig. 1. Temperature profile of hot corrosion test.

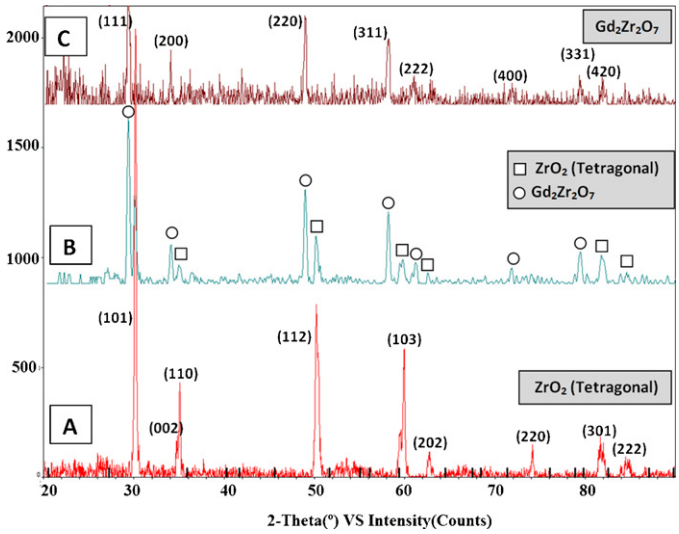

Fig. 2. XRD patterns of as-received (A) YSZ, (B) $Gd_2Zr_2O_7$ + YSZ, and (C) $Gd_2Zr_2O_7$.

2. Material and methods

Nickel-based superalloy (Inconel 738) disks of ∅ 25 mm × 1.5 mm were employed as the substrates. TBCs with a ceramic top coating and a NiCrAlY bond coat (Amdry 9625, Sulzer Metco, particle size 45–75 μm) were deposited onto the superalloy substrates by the atmospheric plasma spray (APS) process. Three types of top coats, YSZ, 50 wt% YSZ + 50 wt% $Gd_2Zr_2O_7$, and $Gd_2Zr_2O_7$ were made using agglomerated powders. The plasma spraying was carried out using a Sulzer-Metco 9 MB plasma spray system with an Ar/H_2 gas mixture. The spraying parameters are given in Table 1. To perform an accelerated high-temperature hot corrosion test on TBCs, a mixture of $Na_2SO_4 + V_2O_5$ deposit was spread onto the surfaces of the TBC specimens with a salt amount of 20 mg/cm^2. The specimens were then set in an electric furnace with an ambient atmosphere under a maximum temperature of 1050 °C for 4 h, Fig. 1. After each 4 h of testing at 1050 °C, the samples were allowed to cool down inside the furnace, and then the coatings were inspected using optical microscope for possible crack initiation. The samples were then recoated with the $Na_2SO_4 + V_2O_5$ salt mixture and the heating profile was repeated until the failure of the coatings.

The morphology and microstructure of the as-sprayed TBC coatings and the coatings after the hot corrosion tests were examined using field emission scanning electron microscopy (Quanta 3D FEG, FEI Company, USA). For surface morphology studies using SEM, a thin Pt layer was sputtered onto the samples to improve the electrical conductivity. To obtain the cross-section SEM images, the specimens were mounted in epoxy resin first before they were sectioned using a slow speed diamond cutter. Subsequently the cross sections were polished using a diamond paste. X-ray diffraction (MiniFlex XRD, Rigaku Corporation, Japan) with Cu Kα radiation λ = 1.54178 Å at a scan speed of 1°/min was used to establish the phase composition of the coatings.

3. Results and discussion

Fig. 2 reveals the X-ray diffraction patterns for the as-received APS YSZ, $Gd_2Zr_2O_7$ + YSZ, and $Gd_2Zr_2O_7$ coatings. It can be seen that the major phase of the APS coated YSZ is tetragonal zirconia. $Gd_2Zr_2O_7$ + YSZ coating includes both tetragonal ZrO_2 and $Gd_2Zr_2O_7$ phases, and $Gd_2Zr_2O_7$ has a single phase as expected. The cross-sectional microstructure of APS YSZ, $Gd_2Zr_2O_7$ + YSZ and $Gd_2Z_2O_7$ TBC specimens are shown in Fig. 3. All layers of the as-sprayed specimens have similar microstructures with a noticeable level of porosity without any visible cracks. For the as-sprayed TBC samples, no delamination can be found along the YSZ/$Gd_2Zr_2O_7$ + YSZ/$Gd_2Zr_2O_7$ top layer and the NiCrAlY bond coat interface. Fig. 4 shows the XRD patterns obtained from the YSZ, $Gd_2Zr_2O_7$ + YSZ, and $Gd_2Z_2O_7$ coatings after the hot corrosion test using the $Na_2SO_4 + V_2O_5$ salt mixture at 1050 °C. Comparing the patterns of the as-sprayed TBC samples, most of the tetragonal zirconia in the YSZ sample has changed to the monoclinic phase and YVO_4 is formed as a hot corrosion product, while for the other two specimens, besides monoclinic ZrO_2 the newly evolved peaks are related to $GdVO_4$.

Typical surface morphologies of YSZ, $Gd_2Zr_2O_7$ + YSZ and $Gd_2Zr_2O_7$ specimens after hot corrosion tests are presented in Fig. 5, with the apparent formation of new crystals. Apart from XRD analysis, Fig. 4, Energy Dispersive Spectroscopy (EDS)

Table 1
Plasma spraying parameters.

Layer	Arc current (A)	Coating distance (mm)	Plasma gas Ar/H_2 (SCFH)	Carrier gas Ar (SCFH)	Powder feed rate (g/min)
Bond coat	500	130	96/15	8	40
Ceramic layer	660	80	64/32	8.4	40

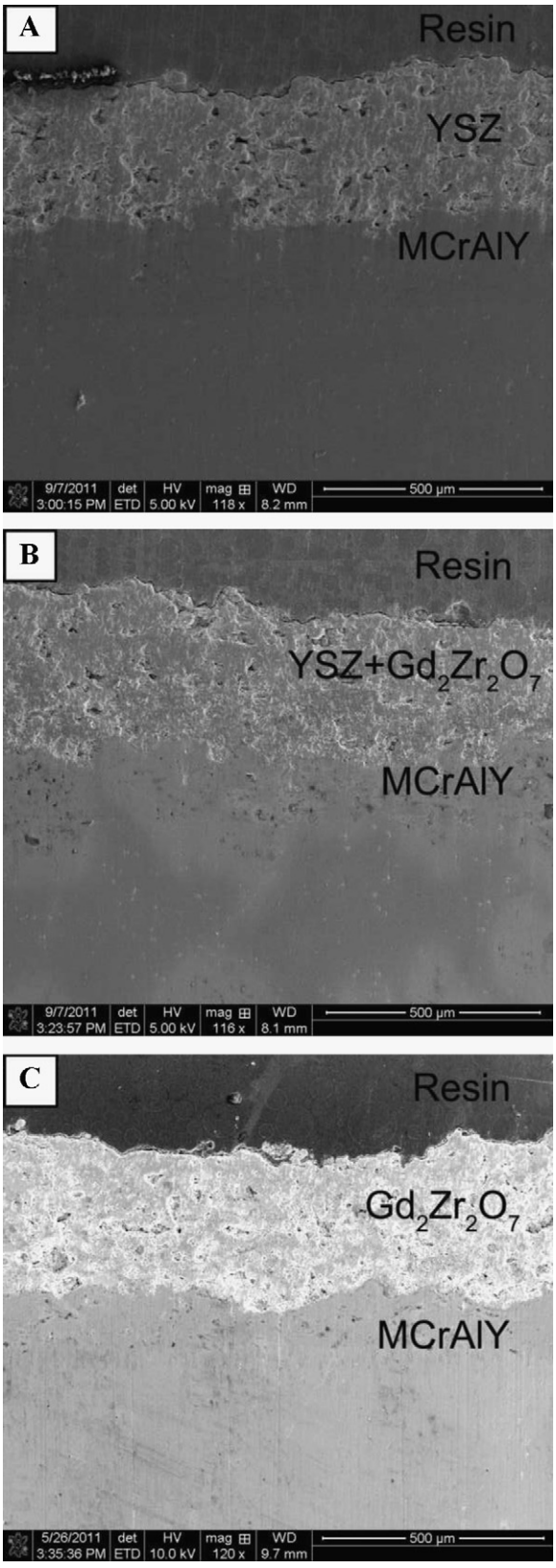

Fig. 3. Cross-section of APS coatings (A) YSZ, (B) $Gd_2Zr_2O_7$ + YSZ, and (C) $Gd_2Zr_2O_7$.

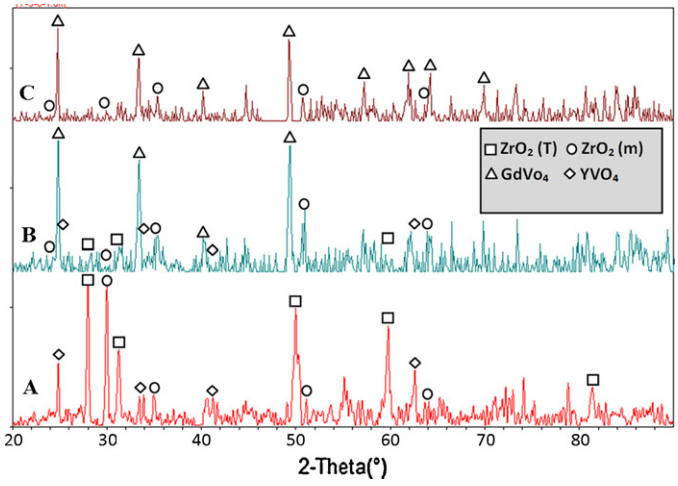

Fig. 4. XRD patterns of (A) YSZ, (B) $Gd_2Zr_2O_7$ + YSZ, and (C) $Gd_2Zr_2O_7$ after hot corrosion in $Na_2SO_4 + V_2O_5$ at 1050 °C.

analysis was performed at different regions of the TBC surfaces to confirm the chemical compositions of the hot corrosion products, Fig. 6. For region A in Fig. 5A, EDS analysis demonstrated that the crystals were composed of yttrium, vanadium, and oxygen. Further XRD analysis confirmed these crystals were YVO_4. For regions A and B in Fig. 5C, the EDS spectra confirmed the presence of $GdVO_4$ (region A) and $Gd_2Zr_2O_7$ (region B). For the region A in Fig. 5C, small amount of zirconium coming from the background was also detected (Fig. 6B).

For the conventional YSZ TBC coating, after hot corrosion tests for 20 h at peak temperature of 1050 °C (five 4-h cycles), serious degradation and spallation started to occur, Fig. 5A. Due to the damage caused by $Na_2SO_4 + V_2O_5$, a porous layer was formed on the YSZ coating. Phase analysis results on these porous areas showed that a large amount of tetragonal zirconia on the surfaces of the conventional YSZ top layer had transformed to monoclinic phase due to the depletion of yttria. In addition, large quantity of rod/plate shaped hot corrosion reaction product, YVO_4, was detected on the surface of the conventional YSZ coating. Similar findings have been reported by other researchers.[6,11,12]

For the $Gd_2Zr_2O_7$ + YSZ and $Gd_2Zr_2O_7$ coatings, the corrosion products are $GdVO_4$ and YVO_4 as well as monoclinic ZrO_2. In Fig. 5C, it is obvious that some regions are perfectly intact and the major phase in these areas is still $Gd_2Zr_2O_7$. Compare to YVO_4, the $GdVO_4$ crystals are much smaller in size and quantity and they have a unique dendrite shape. For the YSZ sample, after hot corrosion tests, large quantity of rod/plate shaped YVO_4 crystals is visible on the coating surfaces.

After exposure to molten salt at 1050 °C for 20 h (five 4-h cycle), spallation and delamination started to occur on the conventional YSZ coatings. Chemical degradation of conventional YSZ coatings can be classified as successive occurrence of related chemical reactions during the hot corrosion tests. During the exposure of V_2O_5 and Na_2SO_4 salt mixture at a high temperature (1050 °C), $NaVO_3$ will be formed.

$$V_2O_5 + Na_2SO_4 \rightarrow 2(NaVO_3) + SO_3 \quad (1)$$

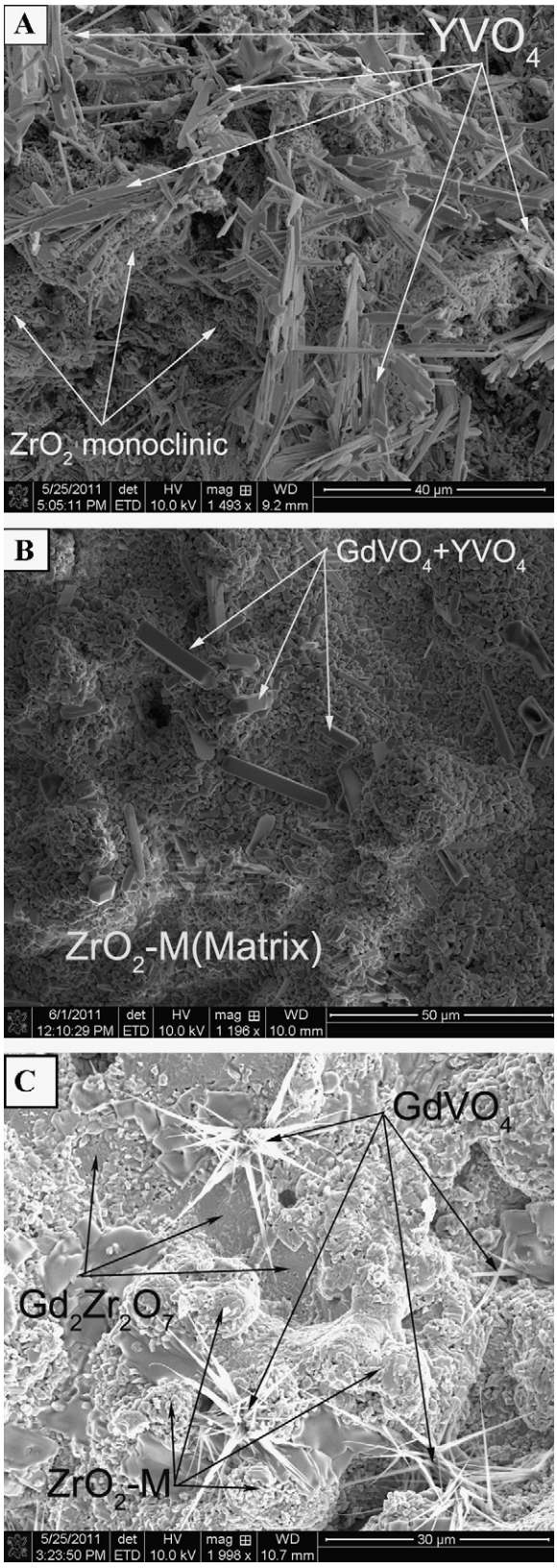

Fig. 5. SEM surface images of (A) YSZ, (B) $Gd_2Zr_2O_7$ + YSZ, and (C) $Gd_2Zr_2O_7$ after hot corrosion in $Na_2SO_4 + V_2O_5$ at 1050 °C.

Then, $NaVO_3$, having a melting point of 610 °C, reacts with yttria from the YSZ solid solution to form YVO_4:

$$ZrO_2(Y_2O_3) + 2(NaVO_3) \rightarrow ZrO_2 + 2(YVO_4) + Na_2O \quad (2)$$

Also Na_2O can react with V_2O_5 directly to form $NaVO_3$:

$$Na_2O\,(\text{base}) + V_2O_5\,(\text{acid}) = 2NaVO_3\,(\text{salt}) \quad (3)$$

For the YSZ sample, after hot corrosion tests, thin rod/plate-like YVO_4 crystals of various sizes are found covering the entire sample surfaces, Fig. 5A. At a temperature above 800 °C, vanadia reacts readily with yttria to from yttrium vanadate[13] and leads to the formation of ZrO_2 monoclinic. The molten $NaVO_3$ is also reported to increase the atom mobility, hence further promote the depletion of yttria from YSZ and the growth of YVO_4 crystals.[3,14,15] The Y^{3+} in the lattice of YSZ has the mobility to migrate preferentially toward the reaction interface due to the high V concentration presented on the coating surfaces.[13] Increasing the reaction time (multiple hot corrosion cycles) enlarges the corroded zones and consequently increases the hot corrosion products. The previously formed YVO_4 crystals may act as nucleation locations for the formation of new crystals, similar to the role of grain boundaries in the nucleation and growth process. Likewise, the repeated charging of molten salts in the hot corrosion tests promotes the formation and growth of the corrosion products due to the increased amount of corrosive species available to react with the coatings. After losing Y_2O_3, the transformation of tetragonal zirconia to monoclinic zirconia during the cooling stage of thermal cycling is accompanied by 3–5% volume expansion, leading to cracking and spallation of TBCs.[6,15–17]

The $Gd_2Zr_2O_7$ + YSZ and $Gd_2Zr_2O_7$ coatings started to degrade after 36 h (nine 4-h cycles) of hot corrosion testing. Exposure of the $Gd_2Zr_2O_7$ + YSZ and $Gd_2Zr_2O_7$ coatings to the molten mixture of $Na_2SO_4 + V_2O_5$ at 1050 °C results in additional peaks on XRD measurements attributed to $GdVO_4$ and monoclinic ZrO_2. As described earlier, Na_2SO_4 and V_2O_5 would first react and form $NaVO_3$, then, the possible reactions that would have produced those identified reaction products include:

$$Gd_2Zr_2O_7\,(s) + 2NaVO_3\,(l) \rightarrow 2GdVO_4\,(s) + 2ZrO_2\,(\text{monoclinic}) + Na_2O \quad (4)$$

$$Gd_2O_3\,(s) + 2NaVO_3\,(l) \rightarrow 2GdVO_4\,(s) + Na_2O \quad (5)$$

No evidences from the XRD patterns indicate direct chemical interactions between Na_2SO_4 with YSZ and $Gd_2Zr_2O_7$, thus the chemical reactions between Na_2SO_4 and YSZ and $Gd_2Zr_2O_7$ are believed to be minimum at the elevated temperature of 1050 °C, which has also been reported by other researchers.[18–21]

V_2O_5 may also react with $Gd_2Zr_2O_7$ directly at elevated temperature to form $GdVO_4$, monoclinic ZrO_2 or ZrV_2O_7.[20–23]

$$3V_2O_5\,(l) + Gd_2Zr_2O_7\,(s) \rightarrow 2ZrV_2O_7\,(s) + 2GdVO_4\,(s) \quad (6)$$

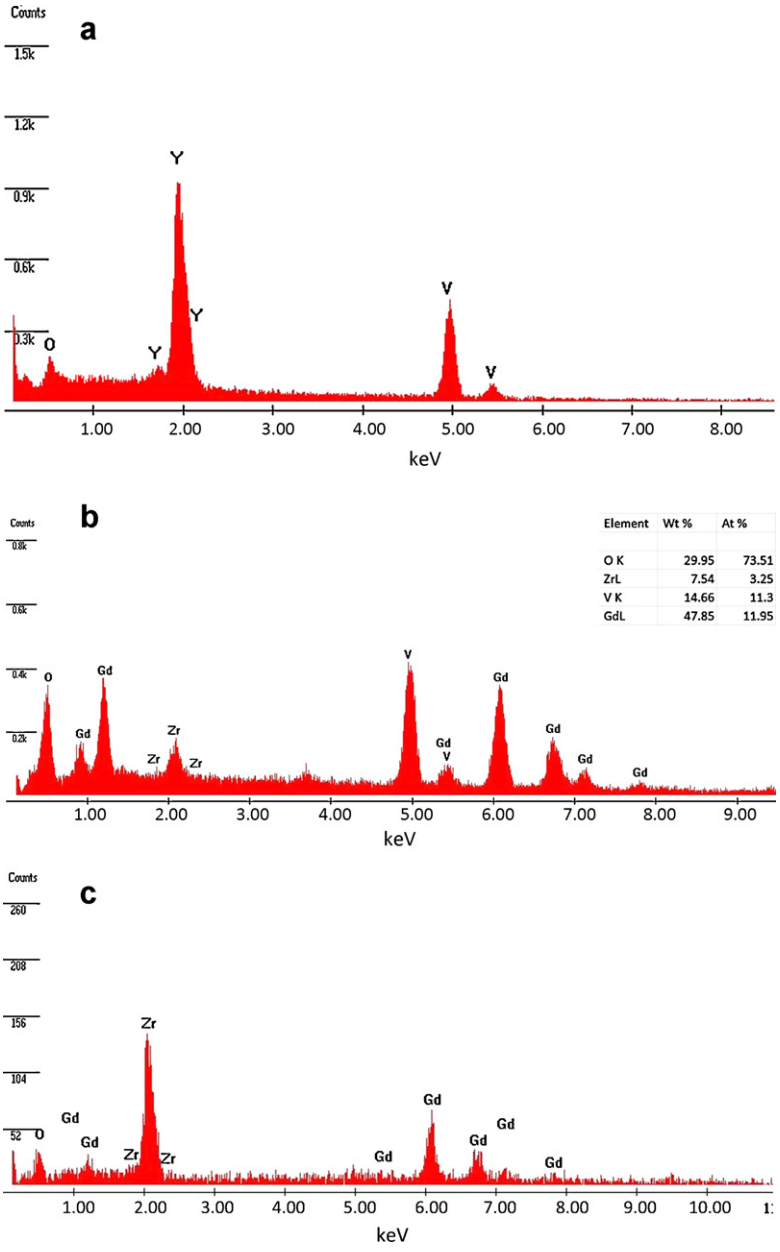

Fig. 6. EDS spectra from the surface of the coatings (A) crystal at region A in Fig. 5A, (B) crystal at region A in Fig. 5C, and (C) region B in Fig. 5C.

$$V_2O_5\,(l) + Gd_2Zr_2O_7\,(s) \rightarrow 2GdVO_4\,(s) + 2ZrO_2\,(\text{monoclinic}) \quad (7)$$

Based on XRD analysis, both $GdVO_4$ and monoclinic ZrO_2 are found in the hot corrosion products of the $Gd_2Zr_2O_7$ coatings; thus reactions (4) and (7) are believed to be the main mechanisms for the degradation of $Gd_2Zr_2O_7$ coatings.

It has been reported that $GdVO_4$ crystals can be produced by the reaction of $Gd_2Zr_2O_7$ and $NaVO_3$ at a temperature as low as 600 °C.[18,19] The production of $GdVO_4$ consumes V_2O_5 and thus postpones the formation of YVO_4 crystals and consequently less monoclinic ZrO_2 and less YVO_4 crystals are formed. This is believed to be the main mechanism for the improved hot corrosion resistance for the $Gd_2Zr_2O_7$ + YSZ composite coating. On the surface of the YSZ + $Gd_2Zr_2O_7$ composite coating, the amount of YVO_4 crystals is significantly less than the amount found in the conventional YSZ coatings. The presence of fine-grained $Gd_2Zr_2O_7$ around YSZ particles also reduces the direct contact of conventional YSZ with molten salt, thus a better corrosion resistance. For pure YSZ coatings, YVO_4 forms throughout the entire surface of the coating. Apart from the stresses induced by the ZrO_2 phase transfer due to the depletion of Y_2O_3, as foreign objects, the corrosion product (YVO_4) could impose extra stresses, which can easily initiate cracks and damage the coating.[18–22] The smaller the YVO_4 size, the lower the stresses and thus a better durability. For the YSZ + $Gd_2Zr_2O_7$

composite coating, after 36 h of accelerated hot corrosion test, many regions in the YSZ + $Gd_2Zr_2O_7$ composite coatings are still intact and the original tetragonal ZrO_2 phases exist. Clearly, YSZ + $Gd_2Zr_2O_7$ composite coating provides a better resistance against hot corrosion than the conventional YSZ. In the $Gd_2Zr_2O_7$ case, the corrosive area is small with isolated dendritic shaped $GdVO_4$ crystals. Also many surface regions remain the original $Gd_2Zr_2O_7$ phase. Unlike the YSZ case, where the hot corrosion attacks the stabilizer Y_2O_3, which has a small quantity in nature, the hot corrosion attacks the bulk $Gd_2Zr_2O_7$ layer, thus the $Gd_2Zr_2O_7$ coating provides a better resistance against hot corrosion than the conventional YSZ.

The reactions between vanadium compounds and ceramic oxides follow a Lewis acid–base mechanism, where the acid vanadium compounds react more readily with the ceramic oxides that have stronger basicity. As reported in literature, the basicity of gadolinium oxide, yttrium oxide, and zirconium dioxide follows the order: $Y_2O_3 > Gd_2O_3 > ZrO_2$, indicating that molten $NaVO_3$ has the tendency to react with Y_2O_3 more easily.[24] Following the nucleation and growth mechanism, at the beginning of the hot corrosion process, the hot corrosion products ($GdVO_4$ and YVO_4) have dendritic like shapes; then as the hot corrosion proceeds, these hot corrosion products become larger and their morphologies change to rod/plate-like shapes. Based on thermodynamic data, $GdVO_4$ is more stable than YVO_4 which indicates a slower $GdVO_4$ growth rate than that of YVO_4 in the prolonged hot corrosion tests. The dendritic shape of $GdVO_4$ shown in Fig. 5C demonstrates that the $Gd_2Zr_2O_7$ coatings have a better hot corrosion resistance than that of YSZ coatings against molten $NaVO_3$. Similar result has been reported by many other researchers using different formation techniques, such as sintering, under different testing temperatures.[14,19,24–27] Hot corrosion resistance was compared qualitatively by measuring the surface areas covered by the hot corrosion products for the three coatings. In Fig. 5A, almost entire surface is covered by the hot corrosion product YVO_4; in Fig. 5B, the area covered by YVO_4 and $GdVO_4$ is estimated to be 20%; and in Fig. 5C, $GdVO_4$ crystal occupies about 5% of the surface area. Fig. 5A was taken after five 4-h hot corrosion cycles and Fig. 5B and C was taken after nine 4-h hot corrosion cycles. Thus it can be concluded that $Gd_2Zr_2O_7$ coatings have a better hot corrosion resistance than that of YSZ coatings against molten $NaVO_3$.

The representative cross section SEM images of the conventional YSZ, $Gd_2Zr_2O_7$ + YSZ, and $Gd_2Zr_2O_7$ coatings after the hot corrosion tests are presented in Fig. 7. As shown in Fig. 7A, the corroded areas near the YSZ/bond coat interface implies a weak coating which can be easily torn off; large harmful horizontal cracks have formed inside the conventional YSZ layer throughout the thickness of the coating. Transverse cracks are clearly visible in the YSZ coating, Fig. 7A. In certain regions, the cracks divided the YSZ layer into several sub-layers, implying the initiation of delamination and spallation of the YSZ coating. Some large cracks have propagated and extended deep into the APS ceramic coat and even reached the top-coat/bond-coat interface, which would be susceptible to cause the debonding of the ceramic coat from the bond coat. Moreover, comparing Figs. 3A and 7A, the thickness of YSZ layer has been reduced

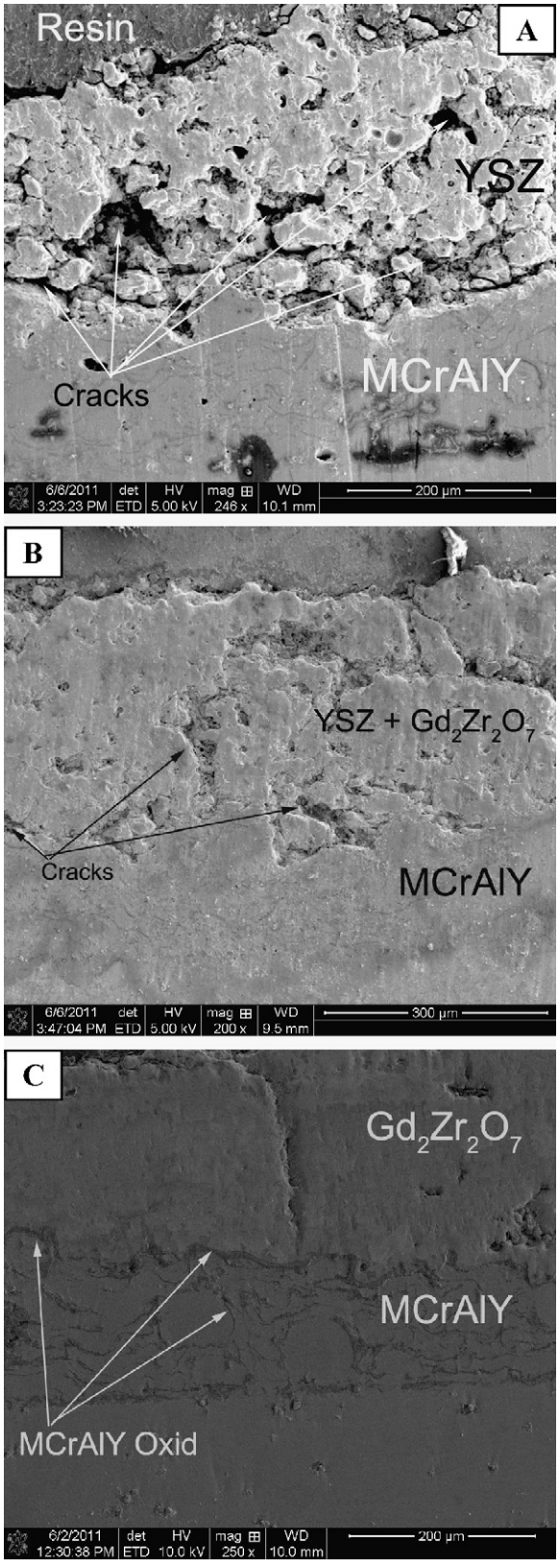

Fig. 7. Cross-section of (A) YSZ, (B) $Gd_2Zr_2O_7$ + YSZ, and (C) $Gd_2Zr_2O_7$ after hot corrosion in $Na_2SO_4 + V_2O_5$ at 1050 °C.

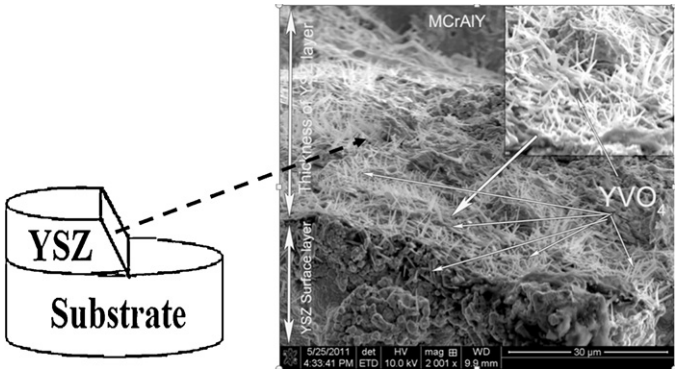

Fig. 8. Cross section along the crack of a delaminated YSZ coating after hot corrosion in $Na_2SO_4 + V_2O_5$ at 1050 °C.

dramatically after the hot corrosion test. Fig. 8 shows the crack of a delaminated YSZ coating. The infiltration of molten salt into the YSZ coating leads to the formation of dendritic YVO_4 crystals throughout the affected thickness of the coating. The formation of YVO_4 crystals implies the depletion of Y_2O_3 in this region, which leads to the subsequent tetragonal to monoclinic ZrO_2 transformation and thus a large destructive volume changes/stresses within the affected layer. The salt attacked YSZ layer can be torn off easily due to the internal stresses during the hot corrosion cycles.

Micro cracks and pores were also observed in $YSZ + Gd_2Zr_2O_7$ coatings, Fig. 7B. In comparison to YSZ sample (Fig. 7A), the $YSZ + Gd_2Zr_2O_7$ coating has finer and fewer micro cracks than the conventional YSZ coating. Fig. 7C shows a $Gd_2Zr_2O_7$ coating cross-section, which has no significant degradation and spallation after hot corrosion test. Although one vertical-crack appears from the surface to bond coat, no visible degradation around the tip of the crack is observed. The cross-section image of the $Gd_2Zr_2O_7$ coating shows less porosity than the conventional YSZ which means it's harder for the molten salts and the oxygen to penetrate through the $Gd_2Zr_2O_7$ layer. This further confirms that the $Gd_2Zr_2O_7$ based coating exhibits a good hot corrosion resistance and good durability.

4. Conclusions

Under a typical gas turbine metal surface temperature of 1050 °C, the reactions between yttria (Y_2O_3) and $V_2O_5/NaVO_3$ produce YVO_4, leaching Y_2O_3 from the YSZ and causing progressive tetragonal to monoclinic destabilization transformation. Based on hot corrosion chemical reaction formulas, the amount of corrosive salt charged in the tests was enough to react with the entire YSZ and $Gd_2Zr_2O_7$ layers (20 mg/cm^2 per cycle). After 20 h (5 cycles) of hot corrosion test at 1050 °C, the failure of the YSZ TBCs has initiated and propagated throughout the entire top coat, and led to the top coat delamination and spallation near the top coat–bond coat interface. The YSZ cross section shows severe macro-cracks and enhanced porosity due to the hot corrosion from the $Na_2SO_4 + V_2O_5$ molten salts. For $YSZ + Gd_2Zr_2O_7$ coating, molten $Na_2SO_4 + V_2O_5$ mixture reacts with $Gd_2Zr_2O_7$ to form $GdVO_4$ and monoclinic ZrO_2. The production of $GdVO_4$ predominately consumes V_2O_5 and thus postpones the formation of YVO_4 crystals and consequently less monoclinic ZrO_2 and less YVO_4 crystals are formed. On the surface of the $YSZ + Gd_2Zr_2O_7$ composite coating, YVO_4 crystals, are significantly smaller (about 20 μm in length) than the large plate shaped YVO_4 found in the conventional YSZ coatings (about 50 μm in length). The presence of fine-grained $Gd_2Zr_2O_7$ around YSZ particles also reduces the direct contact of conventional YSZ with molten salt, thus a better corrosion resistance. Molten $Na_2SO_4 + V_2O_5$ mixture may also react with $Gd_2Zr_2O_7$ coating. However, unlike the YSZ case, where the molten salts attack the stabilizer Y_2O_3, molten $Na_2SO_4 + V_2O_5$ mixture reacts with the bulk $Gd_2Zr_2O_7$ layer to form $GdVO_4$ and monoclinic ZrO_2. Under this accelerated hot corrosion test, bulk $Gd_2Zr_2O_7$ layer started to degrade after 36 h of hot corrosion testing (9 cycles), which is much better than the YSZ case, which started to fail after 5 cycles. The chemical interactions, and the induced phase transformation, are the primary factors for degradation and spallation of the conventional YSZ and $Gd_2Zr_2O_7$ coatings. Based on the degradation rate, the corrosive layer thickness, and the general status of the coating after hot corrosion, $Gd_2Zr_2O_7$ containing coatings have a better hot corrosion resistance at a temperature of 1050 °C than that of YSZ coatings.

Disclaimer

Acknowledgments

This material is based upon work supported by the Department of Energy National Energy Technology Laboratory under Award Number DE-FE0004734 and NASA-EPSCoR program (Grant NNX09AP72A).

References

1. Schulz U, Leyens C, Fritscher K, Peters M, Saruhan-Brings B, Lavigne O, et al. Some recent trends in research and technology of advanced thermal barrier coatings. *Aerosp Sci Technol* 2003;**7**:73–80.
2. Lee JH, Tsai PC, Chang CL. Microstructure and thermal cyclic performance of laser-glazed plasma-sprayed ceria–yttria-stabilized zirconia thermal barrier coatings. *Surf Coat Technol* 2008;**202**:5607–12.

3. Jones RL. Some aspects of the hot corrosion of thermal barrier coatings. *J Therm Spray Technol* 1997;**6**(1):77–84.
4. Han Z, Xu B, Wang H, Zhou S. A comparison of thermal shock behavior between currently plasma spray and supersonic plasma spray CeO_2—Y_2O_3—ZrO_2 graded thermal barrier coatings. *Surf Coat Technol* 2007;**201**:5253–6.
5. Mohan P, Patterson T, Desai VH, Sohn YH. Degradation of free-standing air plasma sprayed CoNiCrAlY coatings by vanadium and phosphorus pentoxides. *Surf Coat Technol* 2008;**203**:427–31.
6. Park SY, Kim JH, Kim MC, Song HS, Park CG. Microscopic observation of degradation behavior in yttria and ceria stabilized zirconia thermal barrier coatings under hot corrosion. *Surf Coat Technol* 2005;**190**:357–65.
7. Chen Z, Wu NQ, Singh J, Mao SX. Effect of Al_2O_3 overlay on hot-corrosion behavior of yttria-stabilized zirconia coating in molten sulfate–vanadate salt. *Thin Solid Films* 2003;**443**:46–52.
8. Rahaman MN, Gross JR, Dutton RE, Wang H. Phase stability, sintering, and thermal conductivity of plasma-sprayed ZrO_2–Gd_2O_3 compositions for potential thermal barrier coating applications. *Acta Mater* 2006;**54**:1615–21.
9. Xu Q, Pan W, Wang J, Wan C, Qi L, Miao H. Rare-earth zirconate ceramics with fluorite structure for thermal barrier coatings. *J Am Ceram Soc* 2006;**89**(1):340–2.
10. Liu ZG, Ouyang JH, Zhou Y, Li J, Xia XL. Densification, structure, and thermophysical properties of ytterbium–gadolinium zirconate ceramics. *Int J Appl Ceram Technol* 2009;**6**(4):485–91.
11. Chen Z, Mabon J, Wen JG, Trice R. Degradation of plasma-sprayed yttria-stabilized zirconia coatings via ingress of vanadium oxide. *J Eur Ceram Soc* 2009;**29**:1647–56.
12. Chen Z, Speakman S, Howe J, Wang H, Porter W, Trice R. Investigation of reactions between vanadium oxide and plasma-sprayed yttria-stabilized zirconia coatings. *J Eur Ceram Soc* 2009;**29**:1403–11.
13. Hertl W. Vanadia reaction with yttria stabilized zirconia. *J Appl Phys* 1988;**63**:5514–20.
14. Jones RL, Williams CE, Jones SR. Reaction of vanadium compounds with ceramic oxides. *J Electrochem Soc* 1986;**33**(1):227–30.
15. Afrasiabi A, Saremi M, Kobayashi A. A comparative study on hot corrosion resistance of three types of thermal barrier coatings: YSZ, YSZ + Al_2O_3 and YSZ/Al_2O_3. *Mater Sci Eng A* 2008;**478**:264–9.
16. Tsai P, Hsu CS. High temperature corrosion resistance and microstructural evaluation of laser-glazed plasma-sprayed zirconia/MCrAlY thermal barrier coatings. *Surf Coat Technol* 2004;**183**:29–34.
17. Gong WB, Sha CK, Sun DQ, Wang WQ. Microstructures and thermal insulation capability of plasma-sprayed nanostructured ceria stabilized zirconia coatings. *Surf Coat Technol* 2006;**201**:3109–15.
18. Xu Z, He L, Mu R, He S, Huang G, Cao X. Hot corrosion behavior of $La_2Zr_2O_7$ with the addition of Y_2O_3 thermal barrier coatings in contacts with vanadate–sulfate salts. *J Alloys Compd* 2010;**504**: 382–5.
19. Xu Z, He L, Mu R, He S, Huang G, Cao X. Hot corrosion behavior of rare earth zirconates and yttria partially stabilized zirconia thermal barrier coatings. *Surf Coat Technol* 2010;**204**:3652–4366.
20. Li S, Liu ZG, Ouyang JH. Hot corrosion behavior of $Yb_2Zr_2O_7$ ceramic coated with V_2O_5 at temperatures of 600–800 °C in air. *Corros Sci* 2010;**52**:3568–72.
21. Liu ZG, Ouyang JH, Zhou Y, Li S. High-temperature hot corrosion behavior of gadolinium zirconate by vanadium pentoxide and sodium sulfate in air. *J Eur Ceram Soc* 2010;**30**:2707–13.
22. Liu ZG, Ouyang JH, Zhou Y, Xia XL. Hot corrosion behavior of V_2O_5-coated $Gd_2Zr_2O_7$ ceramic in air at 700–850 °C. *J Eur Ceram Soc* 2009;**29**:2423–7.
23. Kramer S, Yang J, Levi CG. Infiltration-inhibiting reaction of gadolinium zirconate thermal barrier coatings with CMAS melts. *J Am Ceram Soc* 2008;**91**:576–83.
24. Carre A, Roger F, Varinot C. Study of acid/base properties of oxide, oxide glass, and glass–ceramic surfaces. *J Colloid Interface Sci* 1992;**154**: 174–83.
25. Li S, Liu ZG, Ouyang JH. Study on hot corrosion reactions between $SmYbZr_2O_7$ ceramic and vanadium pentoxide at temperatures of 600–1000 °C in air. *Mater Chem Phys* 2011;**130**:1134–8.
26. Li S, Liu ZG, Ouyang JH. Hot corrosion of $(Sm_{1-x}Yb_x)_2$ Zr_2O_7 ($x = 0$, 0.5, 1.0) ceramics against V_2O_5 molten salt in air at 800 °C. *Int J Appl Ceram Technol* 2011:1–10.
27. Marple BR, Voyer J, Thibodeau M, Nagy DR, Vassen R. Hot Corrosion of lanthanum zirconate and partially stabilized zirconia thermal barrier coatings. *J Eng Gas Turb Power* 2006;**128**:144–52.